

Magnetic tricritical point and nematicity in FeSe under pressure

Rustem Khasanov,^{1,*} Rafael M. Fernandes,² Gediminas Simutis,¹ Zurab Guguchia,^{1,3} Alex Amato,¹ Hubertus Luetkens,¹ Elvezio Morenzoni,¹ Xiaoli Dong,⁴ Fang Zhou,⁴ and Zhongxian Zhao⁴

¹*Laboratory for Muon Spin Spectroscopy, Paul Scherrer Institut, CH-5232 Villigen PSI, Switzerland*

²*University of Minnesota, Minneapolis, MN 55455, USA*

³*Department of Physics, Columbia University, New York, New York 10027, USA*

⁴*Beijing National Laboratory for Condensed Matter Physics, Institute of Physics & University of Chinese Academy of Sciences, CAS, Beijing 100190, China*

Magnetism induced by external pressure (p) was studied in a FeSe crystal sample by means of muon-spin rotation. The magnetic transition changes from second-order to first-order for pressures exceeding the critical value $p_c \simeq 2.4 - 2.5$ GPa. The magnetic ordering temperature (T_N) and the value of the magnetic moment per Fe site (m_{Fe}) increase continuously with increasing pressure, reaching $T_N \simeq 50$ K and $m_{\text{Fe}} \simeq 0.25 \mu_B$ at $p \simeq 2.6$ GPa, respectively. No pronounced features at both $T_N(p)$ and $m_{\text{Fe}}(p)$ are detected at $p \simeq p_c$, thus suggesting that the stripe-type magnetic order in FeSe remains unchanged above and below the critical pressure p_c . A phenomenological model for the (p, T) phase diagram of FeSe reveals that these observations are consistent with a scenario where the nematic transitions of FeSe at low and high pressures are driven by different mechanisms.

I. INTRODUCTION

In unconventional superconductors, like heavy-fermions, cuprates and iron-based materials, superconductivity typically emerges when the antiferromagnetic order of the parent compound is reduced (or fully suppressed) by changing a tuning parameter, such as doping or pressure (see *e.g.* Ref. 1 for a review). The spin-density wave (SDW) antiferromagnetism in iron-based superconductors (Fe-SC's) is, generally, of a stripe-type, *i.e.*, its ordering vector points along one of the two in-plane directions. As a consequence, magnetic order (with the ordering temperature T_N) becomes coupled to a tetragonal-to-orthorhombic structural transition (with the transition temperature T_s). Magnetism occurs in the orthorhombic phase, whereas the paramagnetic phase can be either tetragonal or orthorhombic. Simultaneous magnetic and structural phase transitions ($T_N = T_s$) are observed, *e.g.*, in $\text{Fe}_{1-y}(\text{Se}_x\text{Te}_{1-x})$,² SrFe_2As_2 ,^{3,4} $(\text{Ba}_{1-x}\text{K}_x)\text{Fe}_2\text{As}_2$,⁵ and $\text{Ba}(\text{Fe}_{1-x}\text{Ru}_x)_2\text{As}_2$.⁶ In some Fe-SC families, like Co- or Ni-substituted BaFe_2As_2 ,^{7,8} LaFeAsO ,^{9,10} and NaFeAs ,¹¹ the structural transition precedes the magnetic one by several degrees ($T_N < T_s$). Despite the separation of T_s and T_N , the two transitions are found to follow each other rather closely as a function of tuning parameter for most Fe-SC families, thus suggesting that the structural transition is related to nematic electronic degrees of freedom and that the magnetic fluctuations induce the tetragonal-to-orthorhombic transition at $T_s \gtrsim T_N$.¹²⁻¹⁵

FeSe, a binary pnictide belonging to a broad family of Fe-SC's, represents an exception to the above mentioned rule. Bulk FeSe at ambient pressure undergoes a tetragonal-to-orthorhombic transition at $T_s \simeq 90$ K,¹⁶⁻¹⁹ similarly to the nematic transition of other iron-based parent materials. However, no magnetic order is found to occur at ambient pressure^{18,20-22} and FeSe superconducts below the transition temperature $T_c \simeq 8$ K.¹⁶ While the

absence of a magnetic transition has allowed one to study the pure nematic phase over a wide temperature range, it has also raised the question of whether the nematicity in FeSe has the same magnetic origin as in the other Fe-based families (see *e.g.* Ref. 23 for a review). In contrast to other Fe-SC's,¹⁵ a close relationship between magnetic and nematic fluctuations has not been observed in FeSe, thus suggesting that other degrees of freedom may be at play.^{24,25} From the theory side, a variety of proposals were put forward to explain the mysterious nematicity of FeSe.²⁶⁻³¹

Properties of FeSe, however, change dramatically under applied pressure. T_c rises up to a maximum value of $\simeq 37$ K at $p \simeq 6$ GPa,³²⁻³⁸ and a magnetically ordered phase emerges at $p \simeq 0.8$ GPa.^{21,22} The relation between the magnetic and structural transitions becomes pressure dependent: while T_N rises continuously with increasing pressure,^{21,22} T_s first decreases by reaching $T_s \simeq 20$ K at $p \simeq 1.6$ GPa,³² and then increases again by approaching $T_s \simeq 30$ K at $p \simeq 3$ GPa.^{39,40} It is worth to emphasize, that for $p \lesssim 1.6$ GPa the appearance of magnetism for $p \gtrsim 0.8$ GPa has little influence on the $T_s(p)$ phase boundary thus pointing to an independence of the magnetic and structural transitions in this pressure range. Interestingly, the high-pressure behavior of FeSe resembles the situation observed in other Fe-SC's. Indeed, above $p \simeq 1.6$ GPa the structural and magnetic transitions follow each other,³⁹ and they merge into a combined first-order like transition for pressures exceeding $\simeq 2.2$ GPa.⁴¹

It is quite likely, therefore, that for FeSe the external pressure plays the role of a tuning parameter that changes the driving force of nematicity from a yet to be determined mechanism at low p to the usual magnetic mechanism of other Fe-SC's for pressures exceeding a certain critical value p_c . In order to check the validity of such assumption, muon-spin rotation (μSR) experiments under pressures up to $p \simeq 2.64$ GPa on a FeSe crystal sample were performed. The results obtained in the present study suggest that the magnetic transition

in FeSe changes from second-order for $p \lesssim 2.4$ GPa to first-order for pressures exceeding $p_c \simeq 2.4 - 2.5$ GPa, thus signaling for the occurrence of a magnetic tricritical point. This observation is explained via a phenomenological Ginzburg-Landau model where the nematic transition at low pressures ($p < p_c$) has a different origin than the magnetically-driven vestigial nematicity at higher pressures ($p > p_c$). While other scenarios may also be compatible with this phenomenological model,^{26–30} our findings are consistent with the mechanism proposed in Ref. 31. The renormalization-group calculations presented in that work reveal that the small value of the Fermi energy (which is the case for FeSe at ambient,^{42–45} and at low pressures) makes a d -wave Pomeranchuk transition the leading instability of the system. The magnetism in this case remains weak. Upon increasing the value of the Fermi energy (which for FeSe is presumably accomplished by increasing the pressure) the magnetism becomes the leading instability, and the Pomeranchuk instability is suppressed. In this regime, the nematicity can only arise as a vestigial phase of the magnetically ordered state.

The paper is organized as follows. Sections II A and II B describe the sample preparation procedure and experimental techniques. The results obtained in the zero-field and weak transverse-field μ SR experiments are summarized in Secs. III A and III B. Section IV presents the theoretical phenomenological model describing the emergence of the magnetic tricritical point due to coupled Pomeranchuk and SDW magnetic instabilities. In Section V the dependence of the ordered moment on the magnetic ordering temperature (Sec. V A), the dependence of T_N on pressure (Sec. V B) and the consistency of the second- and the first-order type transitions with the theory (Sec. V C) are discussed. The conclusions follow in Sec. VI.

II. EXPERIMENTAL DETAILS

A. Sample preparation

The FeSe crystal was synthesized by means of floating zone technique as described in Ref. 46. X-ray measurements confirm that the grown cylindrical sample exhibits a single preferred orientation of a tetragonal (101) plane.⁴⁶

B. Experimental Techniques

1. Pressure Cell

The pressure was generated in a double-wall piston-cylinder type of cell made of MP35N alloy. As a pressure transmitting medium 7373 Daphne oil was used. This oil solidifies at $p \simeq 2.3$ GPa at room temperature,⁴⁷ meaning that the experiments for $p < 2.3$ GPa were conducted

in hydrostatic conditions, while for higher pressures the conditions were quasi-hydrostatic.

The pressure was measured in situ by monitoring the pressure induced shift of the superconducting transition temperature of In (pressure indicator). The details of the experimental setup for conducting μ SR under pressure experiments are given in Refs. 48 and 49.

2. Muon-spin rotation

The zero-field (ZF) and weak transverse-field (wTF) muon-spin rotation (μ SR) experiments were carried out at the μ E1 beam line by using the GPD (General Purpose Decay) spectrometer (Paul Scherrer Institute, Switzerland).⁴⁸ Measurements were performed for temperatures ranging from $T \simeq 3$ to $\simeq 120$ K and pressures in the range of $1.7 \leq p \leq 2.64$ GPa. The experimental data were analyzed by using the MUSRFIT package.⁵⁰

The μ SR data were analyzed by decomposing the signal on the sample (s) and the pressure cell (pc) contributions:

$$A(t) = A_s(0)P_s(t) + A_{pc}(0)P_{pc}(t), \quad (1)$$

Here $A_s(0)$ and $A_{pc}(0)$ are the initial asymmetries and $P_s(t)$ and $P_{pc}(t)$ are the muon-spin polarizations belonging to the sample and the pressure cell, respectively. The polarization of the pressure cell $P_{pc}(t)$ was obtained in a separated set of experiments.⁴⁸ In the data analysis the ratio of the component of the pressure cell and the component of the sample $A_s(0)/A_{pc}(0)$ was kept constant for each individual pressure and was always $\approx 80\%$.

The analysis of the ZF- μ SR response of the FeSe sample was made by considering that the magnetic order appears gradually in volume.^{21,22} One part of the muons experiences a static local field corresponding to the magnetic order and the other part stops in nonmagnetic regions:

$$P_s^{\text{ZF}}(t) = m^{\text{ZF}} [f_{\text{osc}} e^{-\lambda_T t} \cos(\gamma_\mu B_{\text{int}} t) + (1 - f_{\text{osc}}) e^{-\lambda_L t}] + (1 - m^{\text{ZF}}) e^{-\lambda_0^{\text{ZF}} t}. \quad (2)$$

Here m^{ZF} is the magnetic volume fraction of the sample, B_{int} is the internal field on the muon stopping site, $\gamma_\mu = 2\pi \cdot 135.5$ MHz/T is the muon gyromagnetic ratio, and λ_T and λ_L are the transverse and the longitudinal exponential relaxation rates, respectively. λ_0^{ZF} is the exponential rate in the non-magnetic parts of the sample. The oscillating (f_{osc}) and non-oscillating ($1 - f_{\text{osc}}$) fractions arise from muons sensing the internal field components which are transversal [$B_{\text{int}} \perp P(0)$] and longitudinal [$B_{\text{int}} \parallel P(0)$] to the initial muon-spin polarization, respectively. Note that since the FeSe crystal sample studied here had one preferable orientation (101 orientation, see Refs. 46,51) the value of $f_{\text{osc}} \simeq 0.75$ was different from that expected for a polycrystalline sample ($f_{\text{osc}} \equiv 2/3$), where all angles between B_{int} and $P(0)$ are equally possible.⁵²

The wTF- μ SR sample response was analyzed considering that the muons stopping in a non-magnetic environment produce long lived oscillations, which reflect the coherent muon-spin precession around the external field B_{ex} .

$$P_s^{\text{wTF}}(t) = (1 - m^{\text{wTF}})e^{-\lambda_0^{\text{wTF}}t} \cos(\gamma_\mu B_{\text{ex}}t + \phi). \quad (3)$$

Here m^{wTF} is the magnetic volume fraction of the sample, ϕ is the initial phase of the muon-spin ensemble and λ_0^{wTF} is the exponential depolarization rate. Note that within the weak transverse-field regime ($B_{\text{ex}} \ll B_{\text{int}}$) and for the short lived oscillations of the muon-spin polarization in magnetically ordered parts of the sample [as is the case for FeSe, see *e.g.* Fig. 1 (a)] one neglects the magnetic contribution.

III. EXPERIMENTAL RESULTS

A. Zero-field μ SR experiments

Figure 1 (a) shows the muon-time spectra at pressures $p \simeq 1.72, 2.21$ and 2.64 GPa. In order to increase the counting statistics (to decrease the error bars) the μ SR spectra accumulated in the temperature range from $\simeq 3$ to 20 K were added. The red lines correspond to the fit of Eq. 1 with the sample contribution described by Eq. 2 to the experimental data. The spontaneous muon-spin precession reflects the appearance of a static magnetic order below the Néel temperature T_N . The field distributions obtained by Fourier transform of the ZF- μ SR spectra are shown in Fig. 1 (b).

From the data presented in Fig. 1 the following points can be concluded: (i) The field distribution in the FeSe sample is well described by a single Lorentzian (see Eq. 2). This suggests that the magnetic order is *commensurate*, which is consistent with earlier μ SR measurements on FeSe polycrystalline samples.^{21,22} (ii) The width of the field distribution is almost pressure independent ($\Delta B_{\text{int}} \simeq 30$ mT). Bearing in mind that the internal field increases with increasing pressure ($B_{\text{int}} \simeq 34, 61, 77$ mT for $p = 1.72, 2.21$, and 2.64 GPa, respectively), this would imply that the magnetic field distribution becomes more homogenous. The distribution of internal fields, and the corresponding ordered magnetic moments per Fe site ($m_{\text{Fe}} \propto B_{\text{int}}$, see *e.g.* Ref. 52), have values $\Delta B_{\text{int}}/B_{\text{int}} = \Delta m_{\text{Fe}}/m_{\text{Fe}} \simeq 45\%, 25\%$, and 19% for $p = 1.72, 2.21$, and 2.64 GPa, respectively. (iii) The increase of the internal field is caused by the corresponding increase of the ordered magnetic moments. Following Ref. 51, where for the stripe-type magnetic order of FeSe the value of $B_{\text{int}} = 0.31 - 0.32$ T per $1 \mu_B$ per Fe atom was determined, the ordered magnetic moment is estimated to be $m_{\text{Fe}} \simeq 0.11, 0.19$, and $0.25 \mu_B$ for $p = 1.72, 2.21$, and 2.64 GPa, respectively.

Figure 2 shows the temperature dependence of the internal field B_{int} and of the magnetic volume fraction m^{ZF}

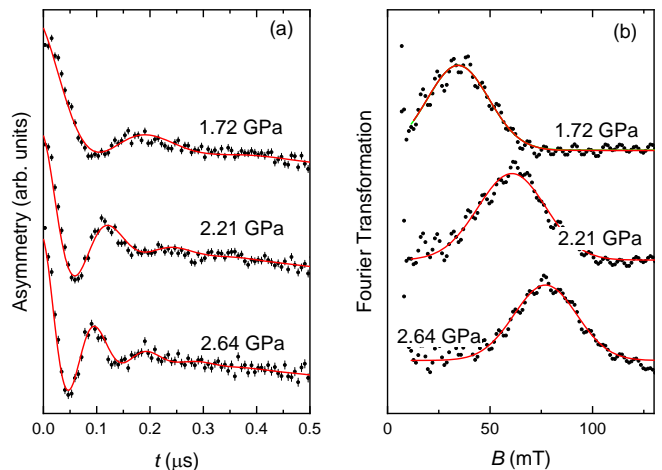


FIG. 1: (a) The muon time spectra collected at pressures $p \simeq 1.72, 2.21$ and 2.64 GPa. The red lines are fits of Eq. 1, with the sample contribution described by Eq. 2 to the experimental data. In order to increase the counting statistics the μ SR spectra accumulated in the temperature range from $\simeq 3$ to 20 K were summed together. (b) The Fourier transform of the ZF- μ SR data shown in the panel (a). The red lines are Lorentzian fits.

obtained from the fit of ZF- μ SR data, for a few characteristic pressures. Obviously, the $B_{\text{int}}(T)$ dependencies at “low” ($p \simeq 1.72$ and 2.21 GPa) and “high” ($p \simeq 2.58$ and 2.64 GPa) pressures are quite different. At low pressures [Fig. 2 (a)], B_{int} appears to decrease continuously with increasing temperature until it vanishes at T_N . This behavior is typical for a second-order transition, which is characterized by a continuous decrease of the order parameter by approaching the critical temperature. In contrast, at higher pressures [Fig. 2 (b)] B_{int} drops abruptly for temperatures slightly above 50 and 52 K for $p = 2.58$ and 2.64 GPa, respectively. This suggests that the transition becomes first-order. Indeed, the fit of the high-pressure data up to $T \simeq 50$ K by means of a power law:

$$B_{\text{int}}(T) = B_{\text{int}}(0) [1 - (T/T_N)^\alpha]^\beta \quad (4)$$

(α and β are the power exponents) suggests that a smooth vanishing of the order parameter in a second order phase transition could be expected around 60 K. Instead an abrupt first order like transition is observed at $T \simeq 50$ K.

The values of the magnetic ordering temperature T_N (except for $p = 2.58$ and 2.64 GPa) and the zero-temperature values of the internal field $B_{\text{int}}(0)$ obtained from the fit of $B_{\text{int}}(T)$ by using Eq. 4 are plotted in Fig. 3. The T_N points for $p = 2.58$ and 2.64 GPa correspond to temperatures where $B_{\text{int}}(T)$ drops to zero [see Fig. 2 (b)]. Figure 3 implies that both T_N and $B_{\text{int}}(0)$ increases linearly with increasing temperature just following the tendency observed in earlier μ SR experiments on polycrystalline FeSe samples.^{21,22} The blue stripe corresponds to the critical pressure p_c where the magnetic transition

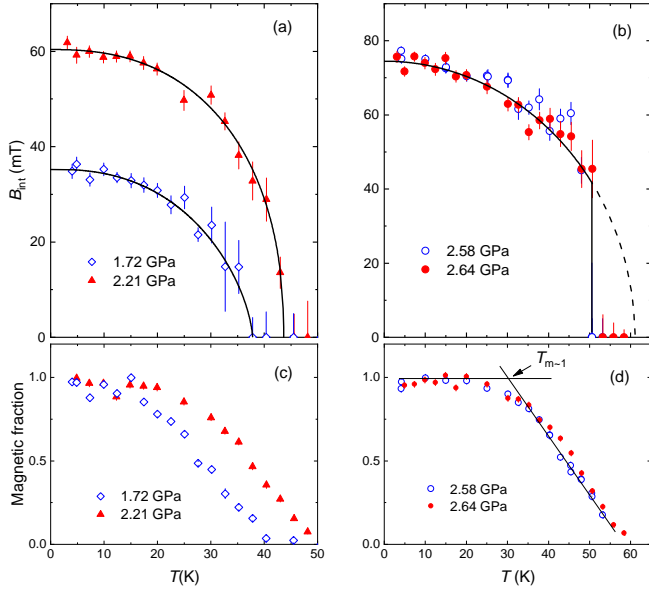


FIG. 2: (a) Temperature dependence of the internal field B_{int} at $p = 1.72$ and 2.21 GPa. (b) The same as in panel (a) but for $p = 2.58$ and 2.64 GPa. The lines in (a) and (b) are fits of Eq. 4 to $B_{\text{int}}(T)$ data. (c) Temperature dependence of the magnetic volume fraction m^{ZF} at $p = 1.72$ and 2.21 GPa. (d) The same as in panel (c) but for $p = 2.58$ and 2.64 GPa. The temperature $T_{m \sim 1}$ (the temperature where the magnetic volume fraction starts to deviate from unity) is determined as a crossing point of $m^{\text{ZF}} = 1$ line with the linear fit of $m^{\text{ZF}}(T)$ in the vicinity of the magnetic transition [panel (d)].

changes from second-order to first-order. It is important to note that T_N and $B_{\text{int}}(0)$ go smoothly through p_c without showing any pronounced features. This indicates that the type of the magnetic order, namely stripe-type magnetism, stays the same above and below the critical pressure p_c .

Our experiments are consistent with other measurements where a change from second-order to first-order transition was observed.^{39,41} Interestingly, the exact values of critical pressure p_c seem to vary between the different experiments. One of the possible reasons for the discrepancy could be a sample-dependence. Also, since the measurements were done in different pressure cells, the degree of hydrostaticity is likely to vary from experiment to experiment. Therefore an alternative explanation is that the critical pressure may depend on the exact stresses in the sample.

B. Weak transverse-field μSR experiments

“Supercooling” and “superheating” across a first-order transition yield metastable states, resulting in hysteresis. In order to search for a possible hysteretic behavior of the magnetic transition in the FeSe crystal sample studied here, wTF- μSR experiments were performed for

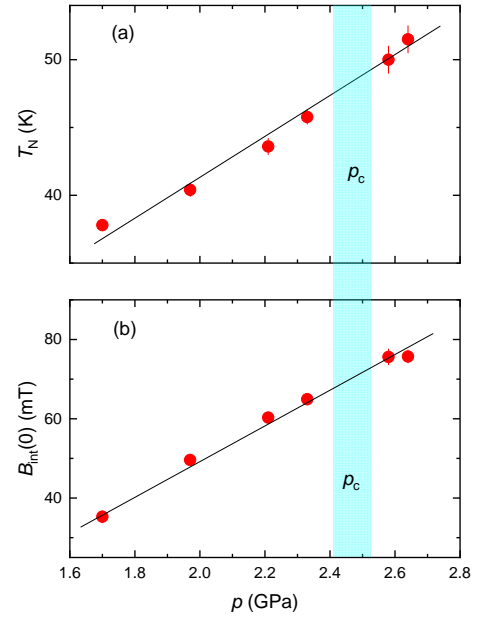


FIG. 3: (a) Pressure dependence of the magnetic ordering temperature T_N obtained from the fit of Eq. 4 to the experimental $B_{\text{int}}(T)$ data. The T_N points for $p = 2.58$ and 2.64 GPa correspond to temperatures where $B_{\text{int}}(T)$ drops to zero [see Fig. 2 (b)]. (b) Pressure dependence of the zero-temperature value of the internal field. The blue stripe represents the pressure region where the magnetic transition changes from second-order to first-order, *i.e.* where a magnetic tricritical point exists.

pressures below (2.05 GPa) and above (2.58 GPa) the critical pressure $p_c \sim 2.4 - 2.5$ GPa (see Fig. 3). Note that the μSR experiments under weak transverse-field applied perpendicular to the muon-spin polarization are a straightforward method to determine the onset of the magnetic transition and the magnetic volume fraction. In this case the contribution to the asymmetry from muons experiencing a vanishing internal spontaneous magnetization can be accurately determined.⁵³

The temperature dependencies of the magnetic volume fraction m^{wTF} obtained from fits of Eq. 1 with the sample contribution described by Eq. 3 to the wTF- μSR data are summarized in Fig. 4. The cooling/warming rates were set to 0.2 K/min. During the warming/cooling process the wTF- μSR spectra were accumulated continuously (5 mins per data point). The solid lines in Fig. 4 correspond to fits of the equation:⁵⁴

$$m^{\text{wTF}}(T)/m^{\text{wTF}}(0) = a(1 + \exp[(T - T_N)/\Delta T_N])^{-1}. \quad (5)$$

Here $m^{\text{wTF}}(0)$ is the magnetic volume fraction at zero-temperature, ΔT_N is the width of the magnetic transition, and a is an adjusting coefficient. The analysis reveals the presence of a small but measurable hysteresis for both pressures. The corresponding $T_N^{\text{up}}/T_N^{\text{down}}$ values are $33.6(3)/34.9(5)$ K and $44.6(6)/46.4(6)$ K for $p = 2.05$ and 2.58 GPa, respectively. This implies that the shift of the

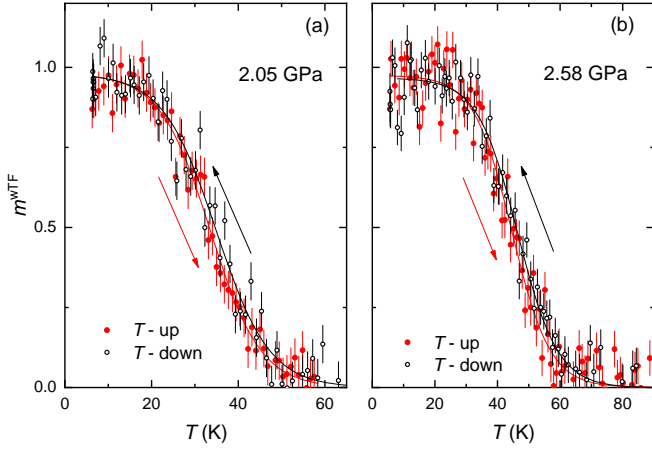


FIG. 4: (a) Temperature evolution of the magnetic volume fraction m^{wTF} of FeSe obtained in the wTF- μ SR measurements at $p = 2.05$ GPa. Closed and open symbols correspond to the experimental data obtained with increasing and decreasing temperature (the sweeping rate is $\simeq 0.2$ K/min, 5 minutes per data point). (b) The same as in (a) but for $p = 2.58$ GPa.

magnetic ordering temperatures [$T_N^{\text{up}} - T_N^{\text{down}} = 1.3(8)$ for $p = 2.05$ GPa and $1.8(8)$ K for $p = 2.58$ GPa] is the same (within the experimental uncertainties) above and below the critical pressure p_c . Bearing in mind that the type of magnetic transition appears to change by crossing p_c (from the second- to the first-order type, see Fig. 2), the similar $T_N^{\text{up}} - T_N^{\text{down}}$ values suggest that the hysteresis observed in our experiments is purely instrumental and is probably caused by difference in thermalization of the pressure cell during warming/cooling procedure.

Note that an approximate 1.5 K hysteresis shift was observed by Wang *et al.*⁴¹ in NMR experiments. Such a temperature shift should be measurable within our experimental accuracy. Further measurements are needed to clarify the reason for the absence of hysteresis in our wTF-experiments.

IV. THEORETICAL MODEL

In this section, we use a general phenomenological model to show that the experimentally observed emergence of the magnetic tricritical point with pressure is consistent with a scenario in which nematicity is driven by different mechanisms at low pressures and at high pressures. Let us denote the nematic order parameter at low pressures by η . For our analysis, while the specific microscopic origin of η is not important, the main point is that it does not arise from the usual Ising-nematic vestigial phase associated with partially melted $\mathbf{Q}_1 = (\pi, 0)$ and $\mathbf{Q}_2 = (0, \pi)$ stripe spin density-wave (SDW). The SDW order parameters associated with these ordering wave-vectors are denoted by \mathbf{M}_1 and \mathbf{M}_2 . Hereafter, to distinguish η from the magnetic-driven nematic order pa-

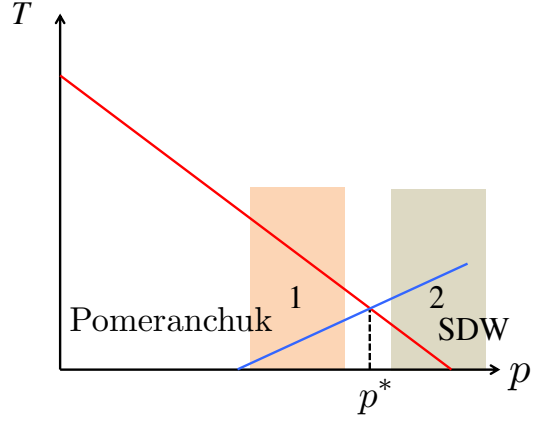


FIG. 5: Schematic (p, T) phase diagram of FeSe used in the phenomenological calculation. The Pomeranchuk and magnetic (SDW) transitions meet at the multi-critical point at (p^*, T_0) . The respective transition temperatures are thus modeled as $T_p = T_0 + \delta$ and $T_m = T_0 - \delta$, with $\delta \propto p^* - p$ such that $\delta > 0$ refers to the Pomeranchuk side and $\delta < 0$ refers to the SDW side.

rameter $M_1^2 - M_2^2$, we will refer to the former as the Pomeranchuk order parameter. The Ginzburg-Landau (GL) free energy of the coupled order parameters is given by (see for instance Refs. 14,31):

$$F[\eta, M_i] = \frac{a_p}{2}\eta^2 + \frac{u_p}{4}\eta^4 + \frac{a_m}{2}(M_1^2 + M_2^2) + \frac{u_m}{4}(M_1^2 + M_2^2)^2 - \frac{g_m}{4}(M_1^2 - M_2^2)^2 - \lambda\eta(M_1^2 - M_2^2) \quad (6)$$

Here, a_p, u_p are the Pomeranchuk GL parameters; a_m, u_m, g_m are the SDW GL parameters; and λ is the coupling constant. To mimic the experimental situation, we assume that pressure suppresses the Pomeranchuk transition and at the same time enhances the SDW transition. This can be modeled by setting $a_p = a_{p,0}(T - T_0 - \delta)$ and $a_m = a_{m,0}(T - T_0 + \delta)$, where $a_{p,0}$ and $a_{m,0}$ are positive prefactors, and T_0 is the mean-field transition temperature in which the Pomeranchuk and magnetic transitions meet. The parameter δ , assumed here to be only pressure dependent, selects the leading instability to be either the Pomeranchuk transition ($\delta > 0$) or the SDW transition ($\delta < 0$). We therefore define the pressure p^* in which the two transitions meet by setting $\delta(p^*) = 0$, implying $\delta \propto p^* - p$. Note that, while we assumed a symmetric change in the transition temperatures with respect to T_0 , the results derived here are more general.

We can now investigate the character of the magnetic transition as δ changes. As shown in Fig. 5, we consider two regions in the regime $p < p^*$ (region 1) and $p > p^*$ (region 2). In region 1, the Pomeranchuk transition happens first at $T_p = T_0 + \delta$. Therefore, we first minimize the GL free energy with respect to the Pomeranchuk order parameter η

$$a_p \eta + u_p \eta^3 = \lambda (M_1^2 - M_2^2) \quad (7)$$

Expanding around the bare Pomeranchuk order parameter $\eta_0 = \sqrt{-\frac{a_p}{u_p}}$ up to quartic order in $M_{1,2}$ and substituting back in Eq. (6), we find the effective SDW free energy:

$$\begin{aligned} \tilde{F}[M_i] = & \frac{a_m}{2} (M_1^2 + M_2^2) - \lambda \eta_0 (M_1^2 - M_2^2) \\ & + \frac{u_m}{4} (M_1^2 + M_2^2)^2 - \frac{1}{4} \left[g_m + \frac{\lambda^2}{(-a_p)} \right] (M_1^2 - M_2^2)^2 \end{aligned} \quad (8)$$

Thus, the onset of Pomeranchuk order has two effects on the SDW degrees of freedom. The first one, arising from the quadratic coefficients, is to select M_1 over M_2 (since we chose $\eta_0 > 0$). This enhances the magnetic transition temperature T_m from $T_m^{(0)} = T_0 - \delta$ to:

$$T_m \approx T_m^{(0)} + 2\delta - \delta^2 \left(\frac{a_{m,0}^2 u_p}{\lambda^2 a_{p,0}} \right) = T_p - \delta^2 \left(\frac{a_{m,0}^2 u_p}{\lambda^2 a_{p,0}} \right) \quad (9)$$

where we expanded to leading orders in δ . The second effect is to suppress the effective quartic coefficient. Setting $M_2 = 0$, the effective quartic coefficient is, for small but finite δ ,

$$\tilde{u}_m \approx u_m - g_m - \frac{1}{\delta^2} \left(\frac{\lambda^4}{a_{m,0}^2 u_p} \right) \quad (10)$$

Thus, for sufficiently small δ , the magnetic transition becomes first order, since \tilde{u}_m becomes negative. This signals the onset of a tricritical point at a pressure p_c slightly below p^* .

To proceed, we now show that the SDW transition remains first-order for $p > p^*$, corresponding to $\delta < 0$ (region 2 of Fig. 5). In this region, because there is no long-range Pomeranchuk order above the magnetic transition, we can use a Gaussian approximation for the Pomeranchuk free energy (as long as $|\delta| \neq 0$). In this case, the Pomeranchuk GL equation is straightforward:

$$\eta = \frac{\lambda}{a_p} (M_1^2 - M_2^2) \quad (11)$$

Substituting this in Eq. (6), we find the effective magnetic free energy:

$$\begin{aligned} \tilde{F}[M_i] = & \frac{a_m}{2} (M_1^2 + M_2^2) + \frac{u_m}{4} (M_1^2 + M_2^2)^2 \\ & - \frac{1}{4} \left(g_m + \frac{2\lambda^2}{a_p} \right) (M_1^2 - M_2^2)^2 \end{aligned} \quad (12)$$

Note that, in contrast to Eq. (8), the magnetic transition is not affected. The only term affected is the quartic coefficient g_m , which becomes, for small but finite $\delta < 0$:

$$\tilde{g}_m = g_m + \frac{\lambda^2}{a_{p,0}(-\delta)} \quad (13)$$

Clearly, g_m gets a large enhancement as the multicritical point is approached. The key point is that the nematic transition in this regime arises as a vestigial order of the magnetic state, via the condensation of the composite order parameter $(M_1^2 - M_2^2)$. This effect can only be captured beyond mean-field. According to the large- N results of Ref. 14, the vestigial Ising-nematic transition and the primary magnetic transitions are simultaneous and first-order for large enough \tilde{g}_m (even if it is still smaller than u_m). In particular, for an anisotropic 3D system with effective dimensionality $2 < d < 3$, the simultaneous first-order transition takes place for $\tilde{g}_m > (3-d)u_m$, which implies, in terms of δ (recall that $\delta < 0$ in region 2):

$$(-\delta) < \frac{\lambda^2}{a_{p,0}} [(3-d)u_m - g_m] \quad (14)$$

Therefore, we conclude that close enough to the tricritical point, the nematic and magnetic transitions are simultaneous and first-order. Note that the results resemble those of Ref. 55, although the models are somewhat different, as in that case the vestigial Ising-nematic transition was not considered.

V. DISCUSSIONS

A. Dependence of the ordered moment on T_N

The internal field at the muon stopping site B_{int} is directly proportional to the value of the ordered magnetic moment.⁵² When the magnetic order is of stripe-type, m_{Fe} scales with B_{int} as: $m_{\text{Fe}} \simeq 3.17 \mu_B/T \times B_{\text{int}}$ (see Ref. 51). The value of the ordered magnetic moment on the Fe site m_{Fe} as a function of the magnetic ordering temperature T_N is shown in Fig. 6. For comparison we have also included m_{Fe} values for various FeSe samples (powders Refs. 21,22 and single crystal Ref. 39) available to date in the literature. Note that due to the small values of m_{Fe} , only μSR experiments permit a determination of m_{Fe} with reliable accuracy. The Mössbauer measurements of Kothapalli *et al.*³⁹ provide $m_{\text{Fe}} \sim 0.2 \mu_B$ for $p = 2.5$ and 4.0 GPa, while the neutron experiments of Bendele *et al.*²² furnished just an upper estimate of $m_{\text{Fe}} \lesssim 0.5 - 0.7 \mu_B$ at $p = 4.4$ GPa.

Figure 6 shows that m_{Fe} scales linearly with T_N . The highest value of the magnetic moment $m_{\text{Fe}} \simeq 0.25 \mu_B$ correspond to the ordering temperature $T_N \simeq 52$ K. The value of m_{Fe} for FeSe obtained in our study is one of the smallest among other mother compounds of Fe-SC families (see *e.g.* Ref. 56 and references therein). It would be important to extend the experiments up to higher pressures (at least up to 4-5 GPa), where according to the

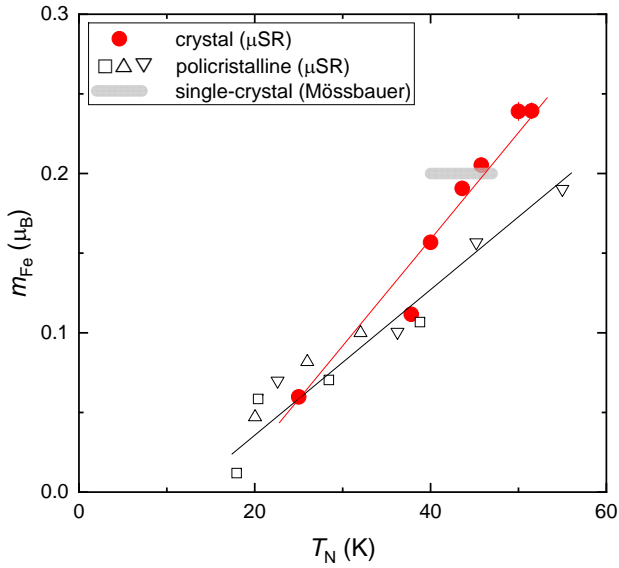


FIG. 6: Value of the ordered magnetic moment on the Fe site m_{Fe} as a function of the magnetic ordering temperature T_N . The red circles correspond to the results of the present study on 101 oriented FeSe crystal. The open squares and the up and down triangles are from $B_{\text{int}}(T_N)$ μSR measurements of Bendele *et al.*^{21,22} on polycrystalline FeSe samples synthesized by two different techniques. The grey stripe correspond to the Mössbauer results of Kothapalli *et al.*³⁹ on high-quality single crystalline FeSe sample. T_N 's for Mössbauer data were obtained by fitting Eq. 4 to the temperature dependence of the hyperfine field H_{pf} at $p = 2.5$ and 3.5 GPa [Fig. 2(b) in Ref. 39]. The solid lines are guides for the eyes.

results of Sun *et al.*⁵⁷ and Böhmer *et al.*⁴⁰ T_N reaches its maximum value. Unfortunately presently our pressure cells do not allow to achieve pressures higher than ~ 2.7 GPa.⁴⁸

B. Pressure dependence of the magnetic ordering temperature

The pressure induced magnetic transition in FeSe was previously studied by μSR ,^{21,22} resistivity,^{57–59} NMR,⁴¹ and Mössbauer experiments.^{39,40} The dependencies of the magnetic ordering temperature on pressure obtained in our studies and the above mentioned experiments are summarized in Fig. 7.

Figure 7 shows that there is a large spread in T_N values obtained by different techniques. The μSR experiments on polycrystalline samples (Refs. 21,22) and crystal (present study) have found the highest T_N values. The NMR measurements, on the other hand, gave the lowest values of T_N .⁴¹ T_N obtained from Mössbauer and resistivity experiments (Refs. 39,40,57–59) lie in between the μSR and NMR data. Another big difference is the width of the magnetic transition. Note that for this one can only compare the μSR and NMR data. There is no criteria to estimate the width of the magnetic transition from

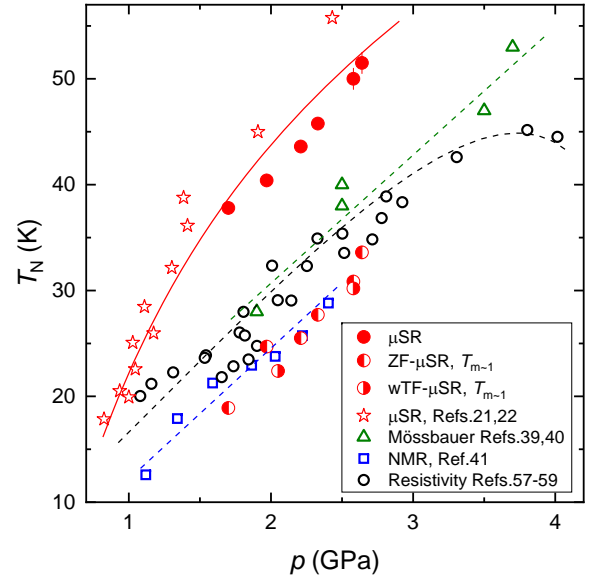


FIG. 7: Dependence of the magnetic ordering temperature (T_N) and the temperature where the magnetic volume fraction starts to decrease below unity ($T_{m \sim 1}$) on applied pressure (p) in FeSe obtained by different techniques. The red closed and semi open circles correspond to the results of the present study on 101 oriented FeSe crystal. The open stars are μSR data on FeSe polycrystalline samples.^{21,22} Open squares and triangles are NMR and Mössbauer data from Refs. 41 and 39, 40, respectively. The open circles correspond to T_N obtained in resistivity experiments.^{57–59} Lines are guides for the eyes.

the resistivity and Mössbauer data. In μSR experiments the magnetic volume fraction m decreases gradually from its maximum value at low temperatures to an almost zero within a rather broad temperature range [~ 20 – 30 K, see Figs. 2 (c), (d) and Fig. 4]. In NMR experiments, however, the magnetic transition, which is associated with an abrupt change of the spectral weight, has at most a 2-3 K transition width.⁴¹

One may determine the temperature $T_{m \sim 1}$ at which the magnetic volume fraction m , as measured in ZF- and wTF- μSR experiments, starts to deviate from unity [see Figs. 2 (c), (d) and Fig. 4]. The criteria for obtaining $T_{m \sim 1}$ is presented in Fig. 2 (d). It is remarkable that the $T_{m \sim 1}$ values plotted in Fig. 7 coincide with the T_N values observed by means of NMR. We believe, therefore, that the spread of T_N shown in Fig. 7 is caused by inhomogeneity of the samples studied.

Indeed, the polycrystalline samples studied previously by μSR (Refs. 21,22) were found to contain some amount of magnetic impurities. This was confirmed by a series of powder neutron diffraction, magnetization and ZF- μSR experiments.^{17,20} The x-ray studies of a crystal, which was grown similarly to the one used in the present study, reveal the presence of the hexagonal impurity phase.⁴⁶ The residual resistance ratio (RRR) was estimated to be $\text{RRR} \simeq 6$. Our ambient pressure ZF- μSR experiments (not shown) reveal an exponential character of the

muon polarization decay which might be explained by a static magnetic field distribution caused by diluted and randomly oriented magnetic moments.²⁰ In contrast, the sample studied by NMR in Ref. 41 was supposed to be much more “clean” with $\text{RRR} \simeq 20$.

Cui *et al.*⁶⁰ proposed that disorder has a dramatic effect on nematicity, particularly near a putative nematic quantum critical point, where finite-size droplets can harbor long-range nematic order in the non-ordered side of the phase transition. This leads to appearance of an *inhomogeneous* nematically-ordered state developing up to higher values of the control parameter (doping or pressure) in comparison with that in a clean (free of impurity) system. Since the nematic order can enhance the magnetic ordering temperature, an inhomogeneous distribution of nematic transition temperatures could cause the observed decrease of the magnetic volume fraction and the increase of T_N .

At this point we would also note that the disorder in FeSe samples has a strong influence not only on the magnetic, but also on the superconducting properties.⁶¹

C. Comparison between the experiment and the theory

The fact that the nematic transition temperature initially decreases with pressure and then increases again once it meets the magnetic transition line suggests that the nematic instability of unpressurized FeSe has a different origin than the nematicity at higher pressures (see also Refs. 23,39,40). Since the phase diagram of FeSe at high pressures is reminiscent of the usual iron-pnictide phase diagram,^{39–41} where nematicity is likely a vestigial phase of the stripe magnetic order,¹⁵ it is expected that the origin of the nematic transition at low pressures involves a different mechanism.

The results presented here of a magnetic tricritical point tuned by pressure allow one to further test this hypothesis. The phenomenological model presented in Sec. IV shows that the emergence of this magnetic tricritical point is not only consistent, but is generally expected if the nematic order parameter at low pressures is different than the vestigial Ising-nematic state arising at high pressures. The model shows that the tricritical point at $p = p_c$ occurs slightly before the magnetic and nematic transition lines meet at $p^* \gtrsim p_c$.

Indeed, our results for pressures up to $p \simeq 2.33$ GPa show that the magnetic order parameter ($B_{\text{int}} \propto m_{\text{Fe}}$) decreases continuously down to zero as temperature increases, which is a clear indication of the second-order transition [see Fig. 2 (a)]. For pressures in the range of $2.33 < p < 2.58$ GPa the magnetic transition changes from second-order to first-order, indicating that the tricritical point at p_c is within this range. Note that the critical pressure values obtained by other techniques are relatively close to the p_c region obtained in our study. The NMR experiments result in $p_c \simeq 2.2$ GPa,⁴¹ while

the Mössbauer data suggest $p_c \gtrsim 2.5$ GPa.³⁹ Finally, for the highest pressures reached in the experiment (2.58 and 2.64 GPa), the magnetic order parameter drops abruptly thus demonstrating that the magnetic transition becomes first-order [Fig. 2 (b)].

Several theoretical models were proposed to explain the unusual nematic order of unpressurized FeSe.^{26–31} While the phenomenological model discussed here does not allow us to distinguish between these different scenarios, our results could be compared with the theory calculations reported in Ref. 31. There, the instabilities of the system towards superconductivity, magnetism, and orbital order were treated on equal footing by a renormalization-group analysis of a general microscopic itinerant model that explicitly takes into account orbital degrees of freedom. The outcome depends on whether energy scale T_{ins} associated with the leading instability is smaller or larger than the Fermi energy E_F . For $T_{\text{ins}} > E_F$, the leading instability is the Pomeranchuk one, followed by s^{+-} superconductivity. For $T_{\text{ins}} < E_F$, the leading instability changes to the magnetic one. Magnetic fluctuations that drive Ising-nematic order also favor a sign-changing s^{+-} superconducting state. The link to the scenario proposed in Ref. 31 assumes that pressure shifts the balance between E_F and T_{ins} in favor of magnetism (and vestigial Ising-nematicity) instead of the non-magnetically ordered Pomeranchuk state. If pressure indeed enhances E_F , it would offer an appealing microscopic mechanism for the phenomenological model proposed in Sec. IV.

VI. CONCLUSIONS

We have performed a detailed study of the pressure-induced magnetic order in the Fe-based binary pnictide superconductor FeSe. Zero-field and weak transverse-field μSR experiments within the pressure range of $1.7 \lesssim p \lesssim 2.64$ GPa on a FeSe crystal sample are presented. Pressure induced magnetic order associated with the appearance of the spontaneous muon-spin precession was detected. The main experimental results are summarized as follows: (i) The value of the ordered magnetic moment per Fe atom (m_{Fe}) increases linearly with increasing pressure, reaching $m_{\text{Fe}} \simeq 0.25 \mu_B$ at $p \simeq 2.6$ GPa. (ii) The magnetic order becomes more homogenous at higher pressures. The distribution of magnetic moments decreases from $\Delta m_{\text{Fe}}/m_{\text{Fe}} \simeq 45\%$ at $p = 1.72$ GPa to $\simeq 19\%$ at $p = 2.64$ GPa.⁶² (iii) The magnetic transition changes from second- to first-order at a critical pressure $p_c \simeq 2.4 - 2.5$ GPa. (iv) Both T_N and m_{Fe} increases linearly with increasing pressure thus suggesting that the stripe-type magnetic order remains unchanged above and below the critical pressure p_c . (v) Comparison of the magnetic ordering temperature T_N with the results presented up to date in the literature suggests that the onset of the magnetic transition in FeSe is determined by the sample homogeneity. In homogenous FeSe samples the

transition into the magnetic state is sharp. In inhomogeneous samples the nematic and magnetic orders may survive locally up to higher temperatures than that expected for the homogeneous sample.

These observations and, in particular, the emergence of a magnetic tricritical point are expected within a scenario where the origin of the nematic transition at high pressures is similar to other Fe-SC's, arising as a vestigial state from the stripe magnetic order. On the other hand, at low pressures, nematicity likely arises from a different mechanism. While this mechanism may still involve magnetic fluctuations, as proposed for instance in Refs. 26,28,31, it remains distinct from the condensation of a composite magnetic order expected near the onset of stripe SDW.

Acknowledgments

This work was performed at the Swiss Muon Source ($S\mu S$), Paul Scherrer Institute (PSI, Switzerland). RMF is supported by the US Department of Energy, Office of Science, Basic Energy Sciences, under Award DE-SC0012336. The work of GS is supported by the Swiss National Science Foundation, grants 200021_149486 and 200021_175935. The work of XD, FZ and ZZ was supported by the "National Key Research and Development Program of China (Grant 2016YFA0300301)", the "Strategic Priority Research Program (B)" of the Chinese Academy of Sciences (Grant XDB07020100) and the Natural Science Foundation of China (Grant 11574370).

-
- * Electronic address: rustem.khasanov@psi.ch
- ¹ D.J. Scalapino, Rev. Mod. Phys. **84**, 1383 (2012).
 - ² S. Li, C. de la Cruz, Q. Huang, Y. Chen, J.W. Lynn, J. Hu, Y.-L. Huang, F.-C. Hsu, K.-W. Yeh, M.-K. Wu, and P. Dai, Phys. Rev. B **79**, 054503 (2009).
 - ³ A. Jesche, N. Caroca-Canales, H. Rosner, H. Borrmann, A. Ormeci, D. Kasinathan, H. H. Klauss, H. Luetkens, R. Khasanov, A. Amato, A. Hoser, K. Kaneko, C. Krellner, and C. Geibel, Phys. Rev. B **78**, 180504(R) (2008).
 - ⁴ J.J. Wu, J.F. Lin, X.C. Wang, Q.Q. Liu, J.L. Zhu, Y.M. Xiao, P. Chow, and C.Q. Jin, Scientific Reports **4**, 3685 (2014).
 - ⁵ S. Avci, O. Chmaissem, D. Y. Chung, S. Rosenkranz, E. A. Goremychkin, J. P. Castellán, I. S. Todorov, J. A. Schlueter, H. Claus, A. Daoud-Aladine, D. D. Khalyavin, M. G. Kanatzidis, and R. Osborn, Phys. Rev. B, **85**, 184507 (2012).
 - ⁶ A. Thaler, N. Ni, A. Kracher, J. Q. Yan, S. L. Bud'ko, and P. C. Canfield, Phys. Rev. B **82**, 014534 (2010).
 - ⁷ N. Ni, A. Thaler, A. Kracher, J. Q. Yan, S. L. Bud'ko, and P. C. Canfield, Phys. Rev. B **80**, 024511 (2009).
 - ⁸ P.C. Canfield and S.L. Bud'ko, Annual Review of Condensed Matter Physics **1**, 27 (2010).
 - ⁹ C. de la Cruz, Q. Huang, J. W. Lynn, Jiying Li, W. Ratcliff II, J. L. Zarestky, H. A. Mook, G. F. Chen, J. L. Luo, N. L. Wang, and P. Dai, Nature, **453**, 899 (2008).
 - ¹⁰ H. Luetkens, H.-H. Klauss, M. Kraken, F.J. Litterst, T. Dellmann, R. Klingeler, C. Hess, R. Khasanov, A. Amato, C. Baines, M. Kosmala, O.J. Schumann, M. Braden, J. Hamann-Borrero, N. Leps, A. Kondrat, G. Behr, J. Werner, and B. Büchner, Nature Materials **8**, 305 (2009).
 - ¹¹ D.R. Parker, M.J.P. Smith, T. Lancaster, A.J. Steele, I. Franke, P.J. Baker, F.L. Pratt, M.J. Pitcher, S.J. Blundell, and S.J. Clarke, Phys. Rev. Lett. **104**, 057007 (2010).
 - ¹² C. Fang, H. Yao, W.-F. Tsai, J. P. Hu, and S. A. Kivelson, Phys. Rev. B **77**, 224509 (2008).
 - ¹³ C. Xu, M. Müller, and S. Sachdev, Phys. Rev. B **78**, 020501(R) (2008).
 - ¹⁴ R. M. Fernandes, A. V. Chubukov, J. Knolle, I. Eremin, J. Schmalian, Phys. Rev. B **85**, 024534 (2012).
 - ¹⁵ R. M. Fernandes, A. E. Böhmer, C. Meingast, and J. Schmalian Phys. Rev. Lett. **111**, 137001 (2013).
 - ¹⁶ F.-C. Hsu, J.-Y. Luo, K.-W. Yeh, T.-K. Chen, T.-W. Huang, P. M. Wu, Y.-C. Lee, Y.-L. Huang, Y.-Y. Chu, D.-C. Yan, and M.-K. Wu, Proc. Natl. Acad. Sci. U.S.A. **105**, 14262 (2008).
 - ¹⁷ E. Pomjakushina, K. Conder, V. Pomjakushin, M. Bende, and R. Khasanov, Phys. Rev. B **80**, 024517 (2009).
 - ¹⁸ T.M. McQueen, A.J. Williams, P.W. Stephens, J. Tao, Y. Zhu, V. Ksenofontov, F. Casper, C. Felser, and R.J. Cava, Phys. Rev. Lett. **103**, 057002 (2009).
 - ¹⁹ R. Khasanov, M. Bende, K. Conder, H. Keller, E. Pomjakushina and V. Pomjakushin, New Journal of Physics **12**, 073024 (2010).
 - ²⁰ R. Khasanov, K. Conder, E. Pomjakushina, A. Amato, C. Baines, Z. Bukowski, J. Karpinski, S. Katrych, H.-H. Klauss, H. Luetkens, A. Shengelaya, and N. D. Zhigadlo, Phys. Rev. B **78**, 220510(R) (2008).
 - ²¹ M. Bende, A. Amato, K. Conder, M. Elender, H. Keller, H.-H. Klauss, H. Luetkens, E. Pomjakushina, A. Raselli, and R. Khasanov, Phys. Rev. Lett. **104**, 087003 (2010).
 - ²² M. Bende, A. Ichsanow, Yu. Pashkevich, L. Keller, Th. Strässle, A. Gusev, E. Pomjakushina, K. Conder, R. Khasanov, and H. Keller, Phys. Rev. B **85**, 064517 (2012).
 - ²³ A.E. Böhmer and A. Kreisel, Journal of Physics: Condensed Matter **30**, 023001 (2017).
 - ²⁴ A. E. Böhmer, T. Arai, F. Hardy, T. Hattori, T. Iye, T. Wolf, H. v. Löhneysen, K. Ishida, and C. Meingast, Phys. Rev. Lett. **114**, 027001 (2015).
 - ²⁵ S.-H. Baek, D.V. Efremov, J.M. Ok, J.S. Kim, J. van den Brink, and B. Büchner, Nature Materials, **14**, 210 (2015).
 - ²⁶ J. K. Glasbrenner, I. I. Mazin, H. O. Jeschke, P. J. Hirschfeld, R. M. Fernandes, and R. Valentí, Nat. Phys. **11**, 953 (2015).
 - ²⁷ R. Yu and Q. Si, Phys. Rev. Lett. **115**, 116401 (2015).
 - ²⁸ F. Wang, S. A. Kivelson, and D.-H. Lee, Nat. Phys. **11**, 959 (2015).
 - ²⁹ Y. Yamakawa, S. Onari, and H. Kontani, Phys. Rev. X **6**, 021032 (2016).
 - ³⁰ L. Fanfarillo, L. Benfatto, and B. Valenzuela, Phys. Rev. B **97**, 121109 (2018).
 - ³¹ A.V. Chubukov, M. Khodas, and R.M. Fernandes, Phys. Rev. X **6**, 041045 (2016).
 - ³² K. Miyoshi, K. Morishita, E. Mutou, M. Kondo, O. Seida, K. Fujiwara, J. Takeuchi, and S. Nishigori, Journal of the Physical Society of Japan **83**, 013702 (2014).

- ³³ Y. Mizuguchi, F. Tomioka, S. Tsuda, T. Yamaguchi, and Y. Takano, *Applied Physics Letters* **93**, 152505 (2008).
- ³⁴ S. Medvedev, T. M. McQueen, I. A. Troyan, T. Palasyuk, M. I. Erements, R. J. Cava, S. Naghavi, F. Casper, V. Ksenofontov, G. Wortmann, and C. Felser, *Nature Mat.* **8**, 630 (2009).
- ³⁵ S. Margadonna, Y. Takabayashi, Y. Ohishi, Y. Mizuguchi, Y. Takano, T. Kagayama, T. Nakagawa, M. Takata, and K. Prassides, *Phys. Rev. B* **80**, 064506 (2009).
- ³⁶ G. Garbarino, A. Sow, P. Lejay, A. Sulpice, P. Toulemonde, M. Mezouar, and M.N. Regueiro, *Europhysics Letters* **86**, 27001 (2009).
- ³⁷ S. Masaki, H. Kotegawa, Y. Hara, H. Tou, K. Murata, Y. Mizuguchi, and Y. Takano, *Journal of the Physical Society of Japan*, **78**, 063704 (2009).
- ³⁸ H. Okabe, N. Takeshita, K. Horigane, T. Muranaka, and J. Akimitsu, *Phys. Rev. B* **81**, 205119 (2010).
- ³⁹ K. Kothapalli, A.E. Böhrer, W.T. Jayasekara, B.G. Ueland, P. Das, A. Sapkota, V. Taufour, Y. Xiao, E. E. Alp, S.L. Bud'ko, P.C. Canfield, A. Kreyssig, and A.I. Goldman, *Nature Communications* **7**, 12728 (2016).
- ⁴⁰ A. E. Böhrer, K. Kothapalli, W.T. Jayasekara, J.M. Wilde, B. Li, A. Sapkota, B.G. Ueland, P. Das, Y. Xiao, W. Bi, J. Zhao, E.E. Alp, S.L. Bud'ko, P.C. Canfield, A.I. Goldman, and A. Kreyssig, *arXiv:1803.09449*, unpublished.
- ⁴¹ P.S. Wang, S.S. Sun, Y. Cui, W.H. Song, T.R. Li, R. Yu, H. Lei, and W. Yu, *Phys. Rev. Lett.* **117**, 237001 (2016).
- ⁴² S. Kasahara, T. Watashige, T. Hanaguri, Y. Kohsaka, T. Yamashita, Y. Shimoyama, Y. Mizukami, R. Endo, H. Ikeda, K. Aoyama, T. Terashima, S. Uji, T. Wolf, H. v. Löhneysen, T. Shibauchi, Y. Matsuda, *Proc. Natl. Acad. Sci. U.S.A.* **111**, 16309 (2014).
- ⁴³ T. Terashima, N. Kikugawa, A. Kiswandhi, E.-S. Choi, J.S. Brooks, S. Kasahara, T. Watashige, H. Ikeda, T. Shibauchi, Y. Matsuda, T. Wolf, A.E. Böhrer, F. Hardy, C. Meingast, H. v. Löhneysen, M.-T. Suzuki, R. Arita, and S. Uji, *Phys. Rev. B* **90**, 144517 (2014).
- ⁴⁴ M. D. Watson, T. K. Kim, A. A. Haghighirad, N. R. Davies, A. McCollam, A. Narayanan, S. F. Blake, Y. L. Chen, S. Ghannadzadeh, A. J. Schofield, M. Hoesch, C. Meingast, T. Wolf, and A. I. Coldea, *Phys. Rev. B* **91**, 155106 (2015).
- ⁴⁵ A. Audouard, F. Duc, L. Drigo, P. Toulemonde, S. Karlsson, P. Strobel, and A.Sulpice, *Europhys. Lett.* **109**, 27003 (2015).
- ⁴⁶ M. Ma, D. Yuan, Y. Wu, H. Zhou, X. Dong, and F. Zhou, *Supercond. Sci. Technol.* **27**, 122001 (2014).
- ⁴⁷ K. Murata, H. Yoshino, H.O. Yadev, Y. Honda, and N. Shirakawa, *Rev. Sci. Instrum.* **68**, 2490 (1997).
- ⁴⁸ R. Khasanov, Z. Guguchia, A. Maisuradze, D. Andreica, M. Elender, A. Raselli, Z. Shermadini, T. Goko, E. Morenzoni, A. Amato, *High Pressure Res.* **36**, 140 (2016).
- ⁴⁹ Z. Shermadini, R. Khasanov, M. Elender, G. Simutis, Z. Guguchia, K.V. Kamenev, A. Amato, *High Pressure Res.* **37**, 449 (2017).
- ⁵⁰ A. Suter and B. M. Wojek, *Phys. Procedia* **30**, 69 (2012).
- ⁵¹ R. Khasanov, Z. Guguchia, A. Amato, E. Morenzoni, X. Dong, F. Zhou, and Z. Zhao, *Phys. Rev. B* **95**, 180504(R) (2017).
- ⁵² A. Yaouanc, and P. Dalmas de Réotier, *Muon Spin Rotation, Relaxation and Resonance: Applications to Condensed Matter* (Oxford University Press, Oxford, 2011).
- ⁵³ R. Khasanov, Z. Guguchia, I. Eremin, H. Luetkens, A. Amato, P.K. Biswas, C. Rüegg, M.A. Susner, A.S. Sefat, N.D. Zhigadlo, and E. Morenzoni, *Sci. Rep.* **5**, 13788 (2015).
- ⁵⁴ R. Khasanov, A. Shengelaya, D. Di Castro, E. Morenzoni, A. Maisuradze, I. M. Savic, K. Conder, E. Pomjakushina, A. Bussmann-Holder, and H. Keller, *Phys. Rev. Lett.* **101**, 077001 (2008).
- ⁵⁵ A. Cano, M. Civelli, I. Eremin, and I. Paul, *Phys. Rev. B* **82**, 020408(R) (2010).
- ⁵⁶ P. Dai, *Rev. Mod. Phys.* **87**, 855 (2015).
- ⁵⁷ J.P. Sun, K. Matsuura, G.Z. Ye, Y. Mizukami, M. Shimozaawa, K. Matsubayashi, M. Yamashita, T. Watashige, S. Kasahara, Y. Matsuda, J.-Q. Yan, B.C. Sales, Y. Uwatoko, J.-G. Cheng, and T. Shibauchi, *Nature Communications* **7**, 12146 (2016).
- ⁵⁸ T. Terashima, N. Kikugawa, S. Kasahara, T. Watashige, T. Shibauchi, Y. Matsuda, T. Wolf, A.E. Böhrer, F. Hardy, C. Meingast, H.v. Löhneysen, and S. Uji, *J. Phys. Soc. Jpn.* **84**, 063701 (2015).
- ⁵⁹ T. Terashima, N. Kikugawa, A. Kiswandhi, D. Graf, E.-S. Choi, J.S. Brooks, S. Kasahara, T. Watashige, Y. Matsuda, T. Shibauchi, T. Wolf, A.E. Böhrer, F. Hardy, C. Meingast, H.v. Löhneysen, and S. Uji, *Phys. Rev. B* **93**, 094505 (2016).
- ⁶⁰ T. Cui and R.M. Fernandes, *arXiv:1801.01988*, unpublished.
- ⁶¹ S. Rössler, C.-L. Huang, L. Jiao, C. Koz, U. Schwarz, and S. Wirth, *arXiv:1712.07898*, unpublished.
- ⁶² This conclusion is made under the assumption of $\Delta B_{\text{int}} \propto \Delta m_{\text{Fe}}$. The change of ΔB_{int} may also relate to the magnetic structure disorder (domain size distribution, correlation length effects, etc).